PCCP

PAPER

Cite this: *Phys. Chem. Chem. Phys.*, 2014, **16**, 21349

Study of structural, electronic and optical properties of tungsten doped bismuth oxychloride by DFT calculations†

Wenjuan Yang,[a] Yanwei Wen,[a] Rong Chen,[b] Dawen Zeng*[a] and Bin Shan*[ac]

Received 26th June 2014,
Accepted 22nd August 2014

DOI: 10.1039/c4cp02801e

www.rsc.org/pccp

First-principle calculations have been carried out to investigate structural stabilities, electronic structures and optical properties of tungsten doped bismuth oxychloride (BiOCl). The structures of substitutional and interstitial tungsten, and in the form of WO_6-ligand-doped BiOCl are examined. The substitutional and interstitial tungsten doping leads to discrete midgap states within the forbidden band gap, which has an adverse effect on the photocatalytic properties. On the other hand, the WO_6-ligand-doped BiOCl structure induces a continuum of hybridized states in the forbidden gap, which favors transport of electrons and holes and could result in enhancement of visible light activity. In addition, the band gap of WO_6-BiOCl decreases by 0.25 eV with valence band maximum (VBM) shifting upwards compared to that of pure BiOCl. By calculating optical absorption spectra of pure BiOCl and WO_6-ligand-doped BiOCl structure, it is found that the absorption peak of the WO_6-ligand-doped BiOCl structure has a red shift towards visible light compared with that of pure BiOCl, which agrees well with experimental observations. These results reveal the tungsten doped BiOCl system as a promising material in photocatalytic decomposition of organics and water splitting under sunlight irradiation.

Introduction

Semiconductor photocatalysis has emerged as an effective technology for pollutant degradation and water splitting. The critical issue that limits its industrialization stems from lack of high efficient semiconductor photocatalytic materials.[1,2] Bismuth oxychloride (BiOCl) has recently drawn great attention because of its highly efficient photocatalytic performance.[3–7] BiOCl[8] is a member of V–VI–VII ternary layered compounds which has been demonstrated to show superior photocatalytic activity under ultraviolet light irradiation. However, the optical band gap of the pure BiOCl sample is about 3.4 eV,[8–10] which makes only the ultraviolet radiation available and thus leads to poor photocatalytic performance under visible light.

In order to enhance the optical absorption of BiOCl, many strategies have been developed to engineer its band structure, which includes doping of metal elements (Cu,[11,12] Mn,[23] Bi,[13] Ag,[14] Fe,[15] *etc.*), non-metal metal elements (I,[16] C,[17] C and N codoping[18]), co-doping of metal and non-metal metal elements (I and Mn,[19] Fe and Nb[20]), introduction of defects (oxygen vacancy[21] and Bi–O–Bi vacancy[22]) and so on. Among these methods, variable-valence metallic ions have seen some success as doping species in improving the photocatalytic properties of pure BiOCl. Li *et al.*[15] synthesized an Fe/BiOCl sample *via* self-doped reactive ionic liquids, the photocatalytic activity of which was shown to be higher than that of the pure BiOCl sample. Fan *et al.*[23] found that Mn doped BiOCl with oxygen vacancy could narrow the band gap and extend the optical absorption to visible, red and infrared light region based on density functional theory (DFT) + *U* calculations. Tungsten (W) is another promising candidate to be doped into BiOCl owing to its variable valence and earth abundance. As a transition metal compound, tungsten chloride (WCl_6) is widely used as a reactant in the synthesis process of BiOCl.[24] Thus tungsten may naturally exist in the product of BiOCl, which shows wider optical absorption and enhanced photocatalytic performance compared with pure BiOCl without WCl_6 as a reactant.[24] What's more, in alkaline solution tungsten could form WO_6 ligand anion[24,25] ($W^{6+} + 8OH^- \rightarrow WO_6^{6-}$), which may also exist in BiOCl samples. However, the role of tungsten in BiOCl crystals remains unknown and the mechanism that underlies the enhanced photocatalytic activity is not clear, which deserves to be further studied.

[a] *State Key Laboratory of Material Processing and Die and Mould Technology and School of Materials Science and Technology, Huazhong University of Science and Technology, Wuhan, 430074, China. E-mail: bshan@mail.hust.edu.cn, dwzeng@mail.hust.edu.cn; Fax: +86-27-87542857; Tel: +86-27-87542857*

[b] *State Key Laboratory of Digital Manufacturing Equipment and Technology, Huazhong University of Science and Technology, Wuhan, 430074, Hubei, China*

[c] *Department of Materials Science and Engineering, The University of Texas at Dallas, Richardson, Texas, 75080, USA*

† Electronic supplementary information (ESI) available. See DOI: 10.1039/c4cp02801e

In the present study, we investigated structural stabilities, electronic structures and optical absorption of tungsten doped BiOCl both in the elemental form and WO_6 ligand form based on DFT + U calculations. Our results reveal the most probable configurations of substitutional (SubW) and interstitial (IntW) tungsten and WO_6 ligand doped in BiOCl crystal and confirm that the elemental doping of the tungsten atom leads to additional density of states (DOS) within the band gap that do not hybrid with intrinsic bands. For the case of WO_6-ligand-doped BiOCl, it produces hybridized DOS in the forbidden band gap, which favors transportation and migration of electrons and holes. The absorption range of sunlight can be effectively extended by WO_6-ligand doped BiOCl phases. An in-depth comparison of our theoretical absorption result and experimental UV-vis spectrum is presented so as to ascertain the effect of WO_6 ligand doped in BiOCl.

Computational methodology

The DFT + U calculations have been performed to investigate the structural, electronic and optical properties of orthorhombic BiOCl doped with tungsten. The exchange–correlation energy is in the form of Perdew–Burke–Ernzerhof (PBE)[26] with the projected augmented wave potentials (PAW)[27] as implemented in the Vienna Ab initio Simulation Package (VASP).[28,29] Kohn–Sham single electron wave functions are expanded by plane waves with an energy cutoff of 400 eV and a uniform 5 × 5 × 3 Γ centered k-points mesh is utilized to sample the Brillion zone. The atomic coordinates are fully relaxed using the conjugate gradient method[30] until the force on each atom is converged to less than 0.02 eV Å^{-1}. The optimized lattice constants for the unit cell BiOCl (space group: $P4nmm$) are: $a = b = 3.91$ Å and $c = 7.40$ Å, which are in good agreement with the experimental values of $a = b = 3.891$ Å and $c = 7.369$ Å.[31] A supercell of 2 × 2 × 3 is built to minimize the image interactions,[23] corresponding to a tungsten doping concentration of about 0.99 wt%, which is close to the experimental value.

Standard DFT calculations have been previously used to successfully model the structural and electronic properties of the pure BiOCl.[18,40–42] We also confirm that additional DFT-D2 correction to account for the vDw forces has little effect on the electronic properties of BiOCl (shown in Fig. S3, ESI†). However, for the configurations of W doped BiOCl, DFT generally fails to appropriately describe the electronic structure of transition metals such as W with the significant intra-atomic correlation of partially filled 5d electrons. In this study, the DFT + U method is used to account for the strong correlation effect in the transition metal doped BiOCl systems.[32,33] We have set $U = 4$ and $J = 1$ for tungsten atoms according to the literature.[34–38]

The absorption spectrum of BiOCl doped with tungsten was also calculated by the Fermi golden rule within the dipole approximation from PBE wave functions. The imaginary part of the dielectric function due to direct interband transitions is obtained by the following equation:[39]

$$\varepsilon_2(\hbar\omega) = \frac{2e^2\pi}{\Omega\varepsilon_0}\sum_{\kappa,\nu,c}\left|\left\langle\psi_\kappa^c|ur|\psi_\kappa^\nu\right\rangle\right|^2\delta\left(E_\kappa^C - E_\kappa^\nu - E\right)$$

where Ω, ω, υ, ν, and c are the unit-cell volume, photon frequency, the vector defining the polarization of the incident electric field, valence bands, and the conduction bands, respectively. ε_2 is the imaginary part of the dielectric function.

Experimental synthesis and optical characterization of the tungsten doped BiOCl sample

The tungsten doped BiOCl composite was synthesized *via* a solvothermal process using ethylene glycol (EG) without water as a solution. Firstly, 5.5 mmol KCl, 0.085 mmol WCl_6 and 0.002 mol $Bi(NO_3)_3{\cdot}5H_2O$ were dissolved in 50 ml of EG by ultrasonication for about 10 minutes and stirred at the room temperature until all reactants were dissolved. Then 20 mmol urea was added to the solution by stirring until it dissolved fully. When the solution became colorless and clear, it was transferred into 100 ml Teflon-lined stainless steel autoclaves. The autoclaves were sealed and maintained at a constant temperature of 150 °C for 3 hours. The samples were subsequently cooled to ambient temperature naturally in the oven. All generated samples were obtained by filtering and washing with ethanol and deionized water 3–5 times to remove EG and impurity ions. Finally, the samples were dried at 90 °C for 10 hours in the oven. The optical band gaps of the powders were measured from UV-vis diffuse reflection spectra which was obtained on a Lambda 35 UV-vis spectrometer (PerkinElmer Co., Ltd, USA) with a scanning wavelength ranging from 200 nm to 700 nm.

Results and discussion

As SubW and IntW have been previously observed experimentally, these two configurations were considered in our modeling. In addition, a model of WO_6 inserting into the Bi_2O_2 planar structure and substituting the Cl atoms of BiOCl have also been proposed in many studies.[24] The model used to simulate the doping effect is shown in Fig. 1. A BiOCl model with a W atom replacing a Bi atom is named SubW-BiOCl as shown in site I in Fig. 1. Site II refers to a BiOCl model with one W atom inserting into two Bi atoms and named IntW-BiOCl. In actual crystal growth, defects such as oxygen vacancies are also observed in the samples.[21] In Fig. 1(III), a SubW-BiOCl with one oxygen vacancy is considered and could be marked as SubW-BiOCl-O′. Similarly IntW-BiOCl with one oxygen vacancy is denoted as IntW-BiOCl-O′, as shown in Fig. 1(IV). The stable doping site of WO_6 atoms in BiOCl is named WO_6-BiOCl in Fig. 1(V).

Structural stability

Tungsten doping leads to a local structural distortion of BiOCl, which is investigated by analyzing crystal lattice constants and angles. Table 1 shows structural parameters of all configurations. The doped structures are obtained by relaxation of the unit cell to the theoretical equilibrium configurations. According to column 2 to 7 in Table 1, the lattice constants and angles of SubW-BiOCl

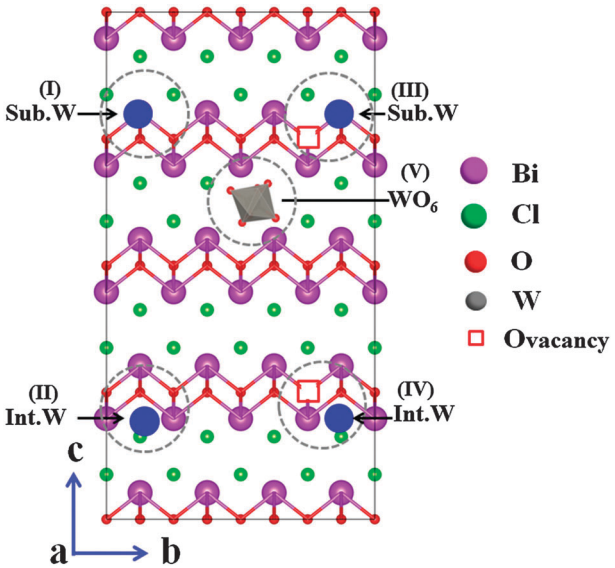

Fig. 1 Optimized crystal models for the W doped BiOCl systems: W doped BiOCl with one Bi atom being substituted by one W atom (I); W doped BiOCl with one W interstitial between two Bi atoms (II); W doped BiOCl with one Bi atom being substituted by one W atom and one oxygen vacancy (III); W doped BiOCl with one W inserting between two Bi atoms and one oxygen vacancy (IV); WO_6 doped BiOCl (V). The green, gray, red, pink balls and red hollow squares represent Cl, W, O, Bi atoms and an oxygen vacancy, respectively.

Table 1 Calculated structural parameters and formation energies for different configurations

Sample	a (Å)	b (Å)	c (Å)	α (°)	β (°)	γ (°)	Formation energy/eV
BiOCl	3.91	3.91	7.40	90	90	90	—
SubW-BiOCl	4.00	4.00	7.42	90	90	90	3.00
IntW-BiOCl	4.00	4.00	7.50	91.3	90.6	89.5	10.46
SubW-BiOCl-O′	3.98	4.08	7.53	93.1	90	90	16.51
IntW-BiOCl-O′	3.94	3.97	7.51	89.3	89.5	90	3.03
WO_6-BiOCl	3.91	3.91	7.65	90	90	90	5.38

and IntW-BiOCl-O′ elongate a little compared with those of pure BiOCl owing to large radius of the W atom than that of the Bi atom. For WO_6-BiOCl, the lattice constant (the last row in Table 1) expands a lot along the c axis owing to the large ligand radius.

The formation energy is an important criterion to evaluate the stability for dopants in the host lattice. The formation energies of tungsten doped BiOCl are calculated using the following equations:

$$E_{f1} = E_{\text{SubW-BiOCl}} - (E_{\text{BiOCl}} - \mu_{\text{Bi}} + \mu_{\text{w}}) \quad (1)$$

$$E_{f2} = E_{\text{IntW-BiOCl}} - (E_{\text{BiOCl}} + \mu_{\text{w}}) \quad (2)$$

$$E_{f3} = E_{\text{SubW-BiOCl-O}'} - (E_{\text{BiOCl}} - \mu_{\text{Bi}} + \mu_{\text{w}} - \mu_{\text{O}}) \quad (3)$$

$$E_{f4} = E_{\text{IntW-BiOCl-O}'} - (E_{\text{BiOCl}} + \mu_{\text{w}} - \mu_{\text{O}}) \quad (4)$$

$$E_{f5} = E_{\text{WO}_6\text{-BiOCl-doped}} - (E_{\text{BiOCl}} - 6\mu_{\text{Cl}} + \mu_{\text{w}} + 6\mu_{\text{O}}) \quad (5)$$

where E_{f1}, E_{f2}, E_{f3}, E_{f4} and E_{f5} are the formation energies of SubW-BiOCl, IntW-BiOCl, SubW-BiOCl-O′, IntW-BiOCl-O′ and WO_6-BiOCl, respectively. The calculated results are listed in the last column of Table 1. E_{BiOCl}, $E_{\text{SubW-BiOCl}}$, $E_{\text{IntW-BiOCl}}$, $E_{\text{SubW-BiOCl-O}'}$, $E_{\text{IntW-BiOCl-O}'}$ and $E_{\text{WO}_6\text{-BiOCl}}$ are the total energies of the pure BiOCl, SubW-BiOCl, IntW-BiOCl, SubW-BiOCl-O′, IntW-BiOCl-O′ and WO_6-BiOCl, respectively. The symbols μ_{Cl}, μ_{Bi}, μ_{O} and μ_{w} represent the chemical potential of the Cl atoms, Bi atoms, O atoms and W atoms, respectively. μ_{Cl} and μ_{O} are determined by the energy of a Cl or an O atom in a Cl_2 gas or an O_2 molecule. μ_{Bi} (μ_{w}) is calculated from the bulk mono Bi (W bcc) crystal. With the absence of oxygen vacancy, the value of SubW-BiOCl is smaller than that of IntW-BiOCl, indicating that the structure of SubW-BiOCl is more stable than IntW-BiOCl. However, with the presence of oxygen vacancy, IntW-BiOCl-O′ becomes more stable than SubW-BiOCl-O′ owing to the fact that oxygen vacancy favors high energy release of IntW-BiOCl structure distortion. The WO_6 ligand can insert into the BiOCl interlayer positions with relatively low energy cost. Thus, SubW-BiOCl, IntW-BiOCl-O′ and WO_6-BiOCl are considered for the following electronic structure investigations.

Electronic properties

The photocatalytic properties of water splitting strongly depend on the electronic structures of semiconductors. To increase the efficiency of the photocatalytic reaction in the region of the visible light, a reasonable band gap of the system is required for the maximum conversion of visible light. Hence, it is important to reduce the band gap so as to shift the spectral response into the visible region and thus improve its photocatalytic properties.

The band structure, total density of states (TDOS) and partial density of states (PDOS) for the pure BiOCl are presented in Fig. 2. The calculated Fermi level is set at an energy of 0 eV in the band gap, indicating typical intrinsic semiconducting characteristics in the electronic structure. Fig. 2 (left and middle) shows that both the conduction band minimum (CBM) and the valence band maximum (VBM) are located at the M and G points in the Brillouin zone, respectively. It implies that the undoped BiOCl is an indirect band gap semiconductor. The calculated band gap is 2.65 eV, which is in consistent with previous DFT calculations,[23,40–42] but smaller than the experimental data of 3.1–3.4 eV.[8,43–45] The underestimation of the band gap value is

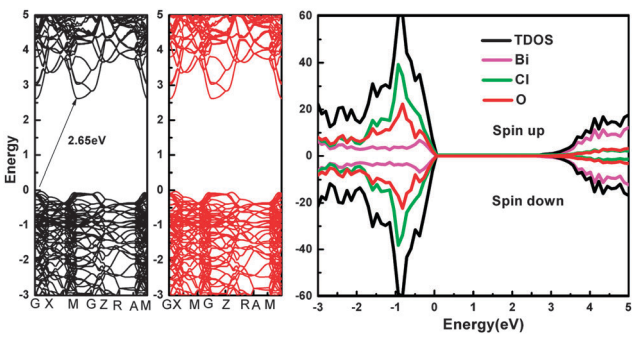

Fig. 2 Band structure (spin up (left) and spin down (middle)) and PDOS (right) for the pure BiOCl. Fermi energy is set at an energy of zero.

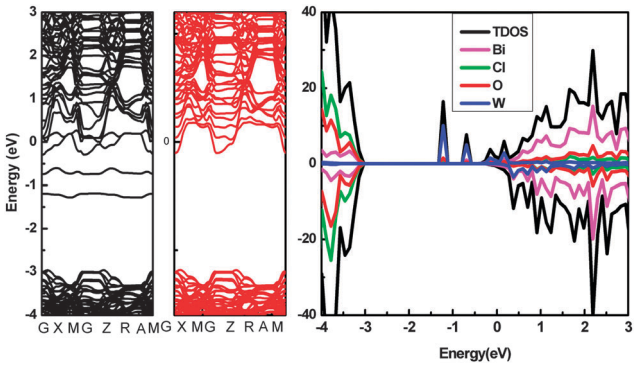

Fig. 3 Band structure (spin up (left) and spin down (middle)) and PDOS (right) for the SubW-BiOCl. Fermi energy is set at an energy of zero.

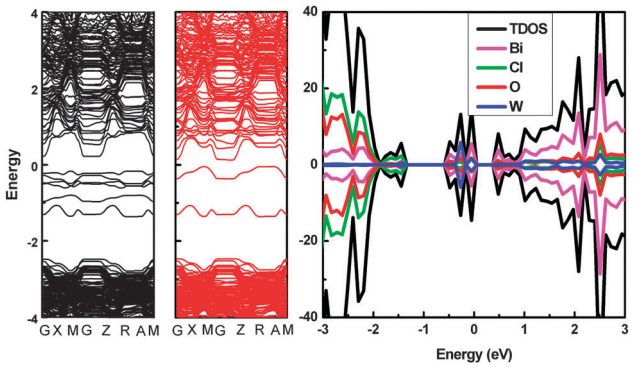

Fig. 4 Band structure (spin up (left) and spin down (middle)) and PDOS (right) for the structure of IntW-BiOCl-O′. Fermi energy is set at an energy of zero.

due to the well-known shortcomings of the exchange–correction function in describing excited states. Although the absolute value of the calculated band gap is not reliable, it could still provide valuable qualitative information on the analysis of the band gap offset. In Fig. 2 (right), the valence band of pure BiOCl is fully occupied, which mainly consists of Cl 2p and O 2p orbitals, whereas the empty conduction band has major contribution from the Bi 6p orbitals.

Fig. 3 depicts the band structure (spin up (left) and spin down (middle)) and DOS structure (right) of SubW-BiOCl. Compared with the undoped BiOCl, a noteworthy feature in the band structure of SubW-BiOCl is the appearance of new impurity energy levels at an energy of around −1.0 eV below Fermi level along with some states at CB tails (Fig. 3(left)). The W dopant increases the asymmetry between the neighbouring atoms and introduces an unpaired d electron. Its 5d states are somewhat delocalized, thus contributing significantly to the formation of impurity energy levels. Furthermore, the Fermi level shifts upward into the conduction band, which makes the structure exhibit a typical n-type metallic character. The intrinsic band gap of this structure is about 2.65 eV, which is nearly the same as that of pure BiOCl. In Fig. 3 (right), the composed orbitals of VBM and CBM are the same as that of pure BiOCl. It can be observed that the Bi 6p orbitals and W $5d^4 6s^2$ orbitals mainly contribute to the mid-gap impurity bands. The DOS in the forbidden gap may serve as electron and hole recombination centers, which are harmful for photocatalytic performance.

Oxygen vacancy, as one of the fundamental and intrinsic defects in semiconductor materials, often has an important impact on their physicochemical properties, such as electronic structures, optical absorption and so on.[46,47] Oxygen vacancy could be easily generated in the growth of BiOCl.[21] Fig. 4 depicts the band structure (spin up (left) and spin down (middle)) and DOS structure (right) of IntW-BiOCl-O′. In Fig. 4 (left), it still presents semiconducting character with a band gap of 2.65 eV along with some states at CB tails. Some isolated impurity states appear around the E-Fermi, similar to that of SubW-BiOCl. In TDOS and PDOS (Fig. 4 (right)), VBM and CBM are mainly composed of Cl 2p states and Bi 6p states, respectively. The gap states have contributions primarily from Bi 6p orbitals and W $5d^4 6s^2$ orbitals, which offer a stepping stone for the absorption of low energy photons *via* the excitation of electrons at the VBM to the intermediate states, from where they can be excited again to the CBM for effective photoactivity of BiOCl. Nevertheless, these gap states can also act as recombination centers of photogenerated carriers, which are not ideal for photocatalytic applications.

To investigate the electronic structure modification of BiOCl by the WO_6 ligand, the band gap and the DOS are presented in Fig. 5. The band structure of WO_6-BiOCl in Fig. 5 (left) displays that semiconductor characterizations are preserved with a band gap of 2.40 eV, which is smaller than that of pure BiOCl. Narrower band gap of WO_6-BiOCl will effectively increase the concentration and lifetime of charge carriers, which favors photocatalytic properties. This band structure introduces continuum bands at an energy of −1.0 eV below Fermi level and hybridizes well with intrinsic bands. This would favor mobility and efficient separation of photoexcited electron–hole pairs. The Fermi level shifts downward, so that WO_6 ligand doped BiOCl shows p-type doping. With respect to the DOS in Fig. 5 (right), the VBM is mainly composed of Cl 2p, O 2p and a small Bi 6p states, whereas the CBM is formed dominantly by Bi 6p, O 2p and a small Cl 2p state. Hybrid bands at an energy of −1.0 eV come from the oxygen of WO_6 as shown in PDOS. We expect that the WO_6-BiOCl structure will exhibit excellent photocatalytic

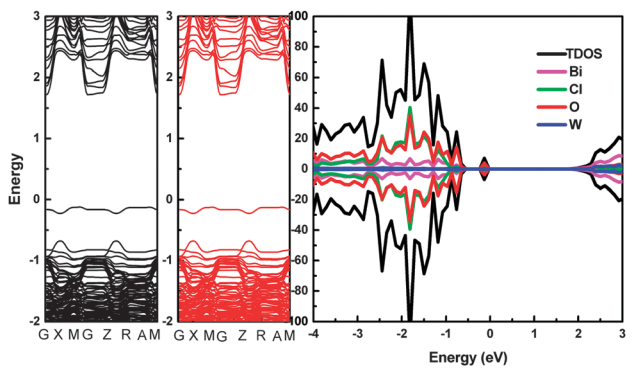

Fig. 5 Band structure (spin up (left) and spin down (middle)) and PDOS (right) of WO_6-BiOCl. Fermi energy is set at an energy of zero.

performance due to the beneficial p-type doping characteristic and band gap reduction without recombination centers.

Band edge positions

Besides appropriate band gaps, suitable CBM and VBM positions of photocatalytic materials are important for the design of a photochemical water reduction and oxidation reaction. The detailed CBM and VBM positions of pure BiOCl, SubW-BiOCl, IntW-BiOCl-O′ and WO_6-BiOCl, TDOS are depicted in Fig. 6. The TDOS and band edges are aligned according to the deep levels which are less sensitive to chemical environments.[48,49] VBM and CBM values with respect to the NHE potential of pure BiOCl (shown in Fig. 7) were taken from the experimental values.[50] For tungsten doped BiOCl, the VBM were obtained according to the relative position difference compared to that of pure BiOCl and the CBM were obtained from the experimental band gap in the DOS figure. The results show that the CBM and VBM positions for the SubW-BiOCl remain the same. However, the isolated impurity bands near the CBM may become recombination centers of photogenerated charge carriers, leading to poor photocatalytic activity. For IntW-BiOCl-O′, the VBM and CBM values also remain unchanged compared to that of pure BiOCl and new isolated impurity states are nearly in the middle of forbidden gap, which may act as the photoexcited electrons and holes recombination centers and reduce the energy conversion efficiency in a photocatalytic process. For the WO_6-BiOCl structure, CBM is identified as unchanged and impurity states in the forbidden gap are not observed. However, VBM shifts upward by 0.25 eV with respect to that of pure BiOCl. Its ability of oxidation is positive enough to oxidize OH^- into $^{\bullet}OH$, which is beneficial for enhancing the photocatalytic properties.

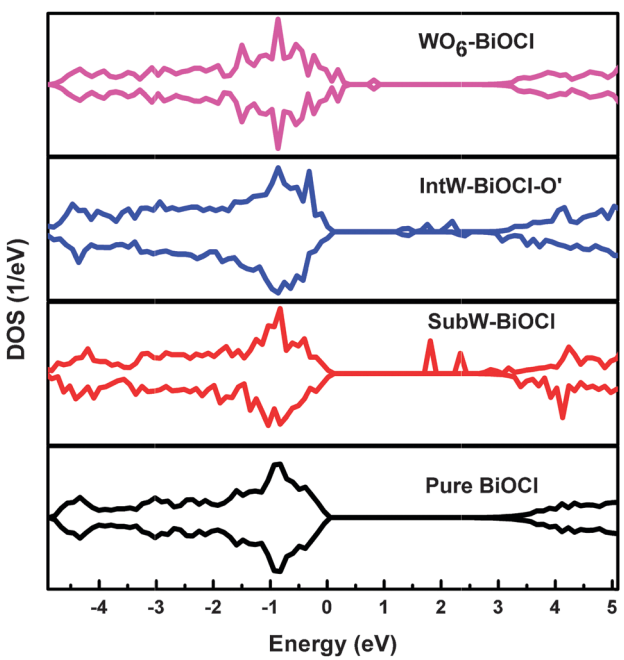

Fig. 6 TDOS for pure BiOCl, SubW-BiOCl, IntW-BiOCl-O′ and WO_6-BiOCl. Deep levels are aligned to get the band edge positions.

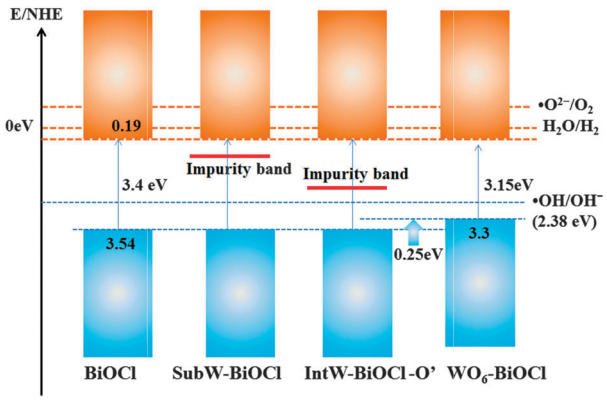

Fig. 7 Comparison of the positions of redox and oxide levels of different configurations. VBM and CBM values are given with respect to the normal hydrogen electrode (NHE) potential.

Charge density differences

Since the structures of SubW-BiOCl and IntW-BiOCl-O′ could yield unhybrid bands which are harmful for photocatalytic performance, we only focus on the structure of WO_6-ligand-doped BiOCl. To evaluate the bonds between the WO_6 ligand and surrounding Bi and O atoms, differential charge density was plotted to identify the bond characteristics of the WO_6-BiOCl structure in Fig. 8. The yellow region represents charge accumulation and the cyan region indicates charge depletion in Fig. 8(a). The transfer of electrons takes place among the O (WO_6 ligand), connected Bi and W atoms. These electrons delocalize around the neighboring Bi and W atoms and accumulate mainly at the nearest O (WO_6 ligand) atoms. The corresponding planar average of the induced charge density difference is shown in Fig. 8(b). The lower charge density at

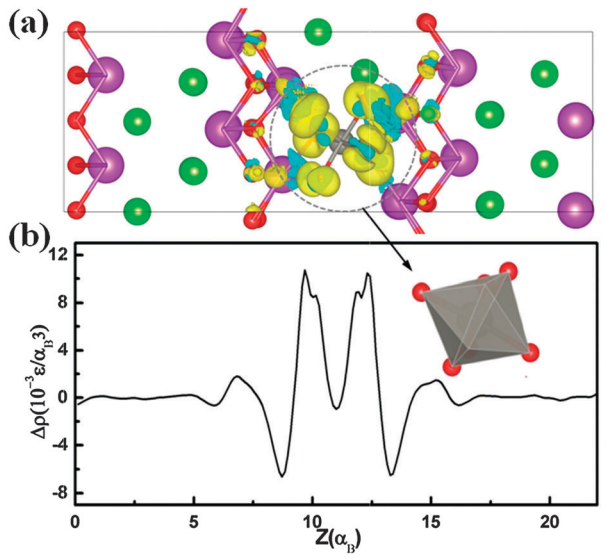

Fig. 8 Differential charge density for the WO_6 doped BiOCl. The yellow region represents charge accumulation and the cyan region indicates charge depletion; the isosurface value is 0.0052079 e $Å^{-3}$ (a). The corresponding planar average of the induced charge density difference for the above structure is plotted in the black line as a function of position in the z direction (b).

the positions of Bi and W atoms illustrates that the transfer of electrons depletes the charges of the Bi and W atoms. And the higher charge density at the O atoms (WO_6 ligand) illustrates that the electrons accumulate at the O atoms. Bi atoms transfer 1.6 electrons to O atoms (WO_6 ligand) according to the Bader charge.[51] The accumulation of charge in the region of the dopant WO_6 ligand also suggests the formation of a chemical bond.

Optical properties

The optical absorption spectra of pure BiOCl and WO_6-BiOCl have been calculated and plotted with an imaginary part of the dielectric function (ε_2) as the y axis in Fig. 9(a). The optical anisotropy for pure BiOCl is in agreement with reported experimental data.[23] For the structure of WO_6-BiOCl, EDX and XPS were performed which shows appearance of characteristic W peaks at the corresponding energy positions (Fig. S1 and S2, ESI†). This demonstrates that W is indeed doped into BiOCl. The intensity of light absorption in the range of 200 nm to 300 nm decreases compared with that of pure BiOCl. And there is a pronounced red shift of the adsorption edge from 380 nm to 410 nm. We calculated the band gap difference of the absorption according to the formula: $E_g = 1240/\lambda$. The energy difference is about 0.25 eV, which agrees well with the band gap narrowing from 2.65 eV to 2.40 eV. We conducted a relative UV-vis absorption experimental test of tungsten doped BiOCl and found the consistency of the red shift of the absorption threshold as shown in the red line (Fig. 9(b)). Moreover, the absorption edge is almost the same as that of the calculated result, indicating reliability of our theoretical model. The red shift of light absorption will excite more electron and hole pairs on the exposed surface of semiconductors and enhance the decomposition of organic pollutants and water splitting.

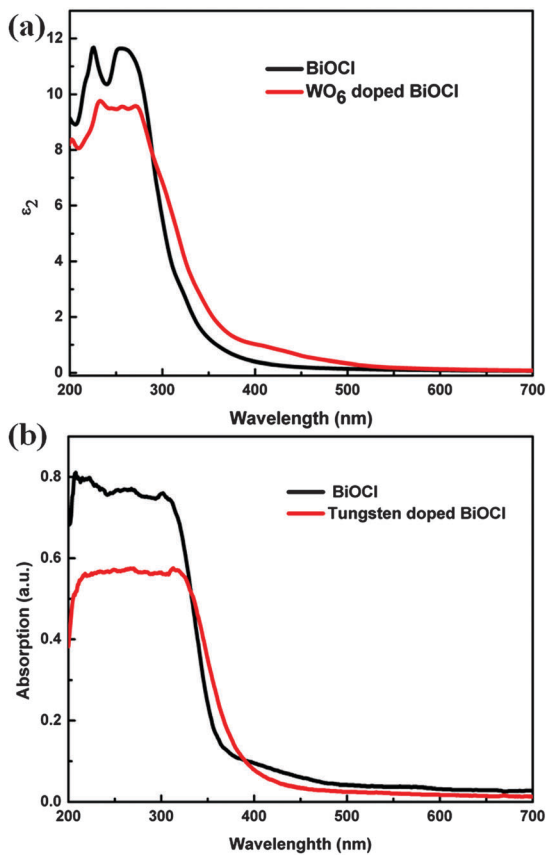

Fig. 9 Calculated optical absorption spectra of pure BiOCl and WO_6 ligand doped BiOCl as a function of wavelength using the DFT + U method. y axis is the imaginary part of the dielectric function (ε_2) (a). Experimental absorption spectra of pure BiOCl and tungsten doped BiOCl (b).

Conclusion

Structural stabilities, electronic properties and optical absorption of SubW-BiOCl, IntW-BiOCl-O′ and WO_6-BiOCl are analyzed by DFT calculations. For the SubW-BiOCl and IntW-BiOCl-O′, these structures will bring up recombination centers in the forbidden gap without tuning positions of the VBM and CBM, which do not facilitate photocatalytic reactions. For the WO_6-BiOCl structure, the band gap decreased by 0.25 eV with mainly VBM shifting upward compared with that of pure BiOCl, which is beneficial for photocatalytic performance. In addition, suitable band edge positions as well as red shift of light absorption render the WO_6-BiOCl structure a suitable and promising photocatalytic material.

Acknowledgements

This work is supported by the National Basic Research Program of China (2013CB934800 and 2011CB606401), National Natural Science Foundation of China (51302094 and 51101064). We thank Jingtian Fang, Bo Ma, Xiao Liu, Bing Zhou, Xueqi Zhou, Xianbao Duan *et al.* for their help. We acknowledge the technology support from the Texas Advanced Computing Center (TACC) at the University of Texas at Austin (http://www.tacc.utexas.edu) for providing grid resources that have contributed to the research results reported within this paper.

Notes and references

1 M. G. Walter, E. L. Warren, J. R. McKone, S. W. Boettcher, Q. Mi, E. A. Santori and N. S. Lewis, *Chem. Rev.*, 2010, **110**, 6446.
2 X. B. Chen, S. H. Shen, L. J. Guo and S. S. Mao, *Chem. Rev.*, 2010, **110**, 6503.
3 X. Zhang, X. B. Wang, L. W. Wang, W. K. Wang, L. L. Long, W. W. Li and H. Q. Yu, *ACS Appl. Mater. Interfaces*, 2014, **6**, 7766.
4 J. M. Ma, X. D. Liu, J. B. Lian, X. C. Duan and W. J. Zheng, *Cryst. Growth Des.*, 2010, **10**, 2522.
5 L. Ye, L. Zan, L. Tian, T. Peng and J. Zhang, *Chem. Commun.*, 2011, **47**, 6951.
6 J. Jiang, K. Zhao, X. Xiao and L. Zhang, *J. Am. Chem. Soc.*, 2012, **134**, 4473.
7 K. Zhao, L. Zhang, J. Wang, Q. Li, W. He and J. J. Yin, *J. Am. Chem. Soc.*, 2013, **135**, 15750.
8 K. L. Zhang, C. M. Liu, F. Q. Huang, C. Zheng and W. D. Wang, *Appl. Catal., B*, 2006, **68**, 125.

9 Y. Q. Lei, G. H. Wang, S. Song, W. Q. Fan and H. J. Zhang, *CrystEngComm*, 2009, **11**, 1857.
10 L. P. Zhu, G. H. Liao, N. C. Bing, L. L. Wang, Y. Yang and H. Y. Xie, *CrystEngComm*, 2010, **12**, 3791.
11 M. Guerrero, S. Pané, B. J. Nelson, M. D. Baró, M. Roldán, J. Sort and E. Pellicer, *Nanoscale*, 2013, **5**, 12542.
12 J. Di, J. X. Xia, S. Yin, H. Xu, X. Li, Y. G. Xu, M. Q. He and H. M. Li, *RSC Adv.*, 2014, **4**, 14281.
13 Y. Yu, C. Y. Cao, H. Liu, P. Li, F. F. Wei, Y. Jiang and W. G. Song, *J. Mater. Chem. A*, 2014, **2**, 1677.
14 W. Xiong, Q. D. Zhao, X. Y. Li and D. K. Zhang, *Catal. Commun.*, 2011, **16**, 229.
15 J. X. Xia, L. Xu, J. Zhang, S. Yin, H. M. Li, H. Xu and J. Di, *CrystEngComm*, 2013, **15**, 10132.
16 K. Zhang, D. Q. Zhang, J. Liu, K. X. Ren, H. Luo, Y. J. Peng, G. S. Li and X. B. Yu, *CrystEngComm*, 2012, **14**, 700.
17 J. Yu, B. Wei, L. Zhu, H. Gao, W. Sun and L. Xu, *Appl. Surf. Sci.*, 2013, **284**, 497.
18 P. Q. Wang, Y. Bai, J. Y. Liu, Z. Fan and Y. Q. Hu, *Micro Nano Lett.*, 2012, **7**, 876.
19 C. D. Wang, H. Qiu, T. Inoue and Q. W. Yao, *Comput. Mater. Sci.*, 2014, **85**, 138.
20 M. Nussbaum, N. Shaham-Waldmann and Y. Paz, *J. Photochem. Photobiol., A*, 2014, **290**, 11.
21 L. Q. Ye, K. J. Deng, F. Xu, L. H. Tian, T. Y. Peng and L. Zan, *Phys. Chem. Chem. Phys.*, 2012, **14**, 82.
22 M. L. Guan, C. Xiao, J. Zhang, S. J. Fan, R. An, Q. M. Cheng, J. F. Xie, M. Zhou, B. J. Ye and Y. Xie, *J. Am. Chem. Soc.*, 2013, **135**, 10411.
23 X. C. Zhang, C. M. Fan, Y. W. Wang, Y. F. Wang, Z. H. Liang and P. D. Han, *Comput. Mater. Sci.*, 2013, **71**, 135.
24 W. J. Yang, B. Ma, W. C. Wang, Y. W. Wen, D. W. Zeng and B. Shan, *Phys. Chem. Chem. Phys.*, 2013, **15**, 19387.
25 Y. S. Xu, Z. J. Zhang and W. D. Zhang, *Dalton Trans.*, 2014, **43**, 3660.
26 J. P. Perdew, K. Burke and M. Ernzerhof, *Phys. Rev. Lett.*, 1996, **77**, 3865.
27 P. E. Blöchl, *Phys. Rev. B: Condens. Matter Mater. Phys.*, 1994, **50**, 17953.
28 G. Kresse and J. Furthmüller, *Comput. Mater. Sci.*, 1996, **6**, 15.
29 G. Kresse and J. Furthmüller, *Phys. Rev. B: Condens. Matter Mater. Phys.*, 1996, **54**, 8245.
30 W. Press, B. Flannery, S. Teukolsky and W. Vetterling, *Numerical Recipes: The Art of Scientific Computing*, Cambridge University Press, New York, 1986.
31 R. W. G. Wyckoff, *Crystal Structures*, Wiley, New York, 1963.
32 A. Houari, S. F. Matar and M. A. Belkhir, *Comput. Mater. Sci.*, 2008, **43**, 392.
33 I. Ahmad and B. Amin, *Comput. Mater. Sci.*, 2013, **68**, 55.
34 W. Zhou, L. J. Liu, M. Y. Yuan, Q. G. Song and P. Wu, *Comput. Mater. Sci.*, 2012, **54**, 109.
35 H. Kamisaka, T. Suenaga, H. Nakamura and K. Yamashita, *J. Phys. Chem. C*, 2010, **114**, 12777.
36 E. Finazzi, C. Di Valentin, G. Pacchioni and A. Selloni, *J. Chem. Phys.*, 2008, **129**, 154113.
37 M. Nolan, S. D. Elliott, J. S. Mulley, R. A. Bennett, M. Basham and P. Mulheran, *Phys. Rev. B: Condens. Matter Mater. Phys.*, 2008, **77**, 235424.
38 B. J. Morgan and G. W. Watson, *Surf. Sci.*, 2007, **601**, 5034.
39 A. J. Read and R. J. Needs, *Phys. Rev. B: Condens. Matter Mater. Phys.*, 1991, **44**, 13071.
40 L. P. Zhu, G. H. Liao, N. C. Bing, L. L. Wang, L. L. Wang, Y. Yang and H. Y. Xie, *CrystEngComm*, 2010, **12**, 3791.
41 Z. Q. Shi, Y. Wang, C. M. Fan, Y. F. Wang and G. Y. Ding, *Trans. Nonferrous Met. Soc. China*, 2011, **21**, 2254.
42 B. Pare, B. Sarwan and S. B. Jonnalagadda, *J. Mol. Struct.*, 2012, **1007**, 196.
43 L. J. Zhao, X. C. Zhang, C. M. Fan, Z. H. Liang and P. D. Han, *Phys. B*, 2012, **407**, 3364.
44 W. L. Huang and Q. S. Zhu, *Comput. Mater. Sci.*, 2008, **43**, 1101.
45 W. L. Huang and Q. S. Zhu, *Comput. Mater. Sci.*, 2009, **46**, 1076.
46 T. Bredow and G. Pacchioni, *Chem. Phys. Lett.*, 2002, **355**, 417.
47 C. T. Campbell and C. H. F. Peden, *Science*, 2005, **309**, 713.
48 J. C. Wu, J. Zheng, P. Wu and R. Xu, *J. Phys. Chem. C*, 2011, **115**, 5675.
49 H. G. Sun, X. Zhao, L. Zhang and W. L. Fan, *J. Phys. Chem. C*, 2011, **115**, 2218.
50 T. B. Li, G. Chen, C. Zhou, Z. Y. Shen, R. C. Jin and J. X. Sun, *Dalton Trans.*, 2011, **40**, 6751.
51 R. Bader, *Atoms in Molecules: A Quantum Theory*, Oxford University Press, New York, 1990.